RSC Advances




ROYAL SOCIETY OF CHEMISTRY

www.rsc.org/advances

Journal Name

COMMUNICATION

# Anti-stacking Dense Conversion of Solid Organic Sodium Salt Particles into Graphene with Excellent Electrode Performance

Received 00th January 20xx,
Accepted 00th January 20xx

DOI: 10.1039/x0xx00000x

www.rsc.org/

H. J. Cui,[ab] Y. Y. Zhu,[ab] J.F. Zheng,*[a] S. P. Jia,[a] Z. J. Wang[a] and Z. P. Zhu*[a]

**Graphene frameworks can be directly converted by a rapid decomposition of common solid organic sodium salts, during which the gases produced simultaneously play a crucial role in resisting the inter-graphene stacking behaviour through an in-situ filling between the growing graphene films. The framework structure endows it with excellent electrode performance.**

The versatile and supreme properties of graphene have highlighted its great potential in revolutionizing numerous existing materials.[1-7] The application of graphene is essentially driven by the progress in their massive production.[1] Actually, graphene, single or few-layers graphite crystals, are rather common structurally, with a hexagonal network structure built by thermodynamically most stable $sp^2$-hybrided carbons. Although nearly all carbon-containing compounds can be converted into $sp^2$-carbons, the first addressing on this common structure was achieved just ten years ago by physical exfoliation of graphite crystals[8] and their mass chemical synthesis still meets a great challenge. This situation is certainly derived from the inherent π-π interaction of graphene films, which normally drives graphene stack as thick graphite crystals. The current top-down strategy for graphene exfoliating from graphite crystal is just based on a compelling breakage of the π-π interaction by physical forces,[8,9] molecule intercalation,[10] or by oxidative intercalation.[11] Although the oxidation exfoliation was fully proved efficient and scalable,[1] the required lengthy oxidation-reduction procedure and the involved environmental problems would lift up production cost greatly. Bottom-up chemical synthesis of graphene from atomic or molecular carbon species has been intensively studied and got much successes, such as the SiC decomposition based epitaxial growth,[12,13] the chemical vapor deposition (CVD) of hydrocarbons,[14-17] the carbonization of organic polymer thin films,[18] and the polymerization and cyclodehydrogenation of molecular monomers.[19,20] These chemical approaches have unique advantages in controlling the size, thickness, and structure of graphene films for diverse applications,[21-25] but they are difficult to support the mass production because the baffling π-π stacking problem was not resolved properly, just bypassed via a strict control in product quantity (performing at quite low carbon density). Additionally, in order to direct two-dimensional (2D) growth of graphene, special substrates were usually employed,[14-18] which additionally uplift synthesis cost because the subsequent graphene transfer or substrate removal is difficulty.[26,27] Here we show that the rapid decomposition of the solid particles of organic sodium salts is capable of directly converting them into core-shell particles constructed with graphene framework (GF) shells and $Na_2CO_3$ cores (Figure 1a). Pure GFs can be readily obtained via removing the $Na_2CO_3$ cores by simply washing with water. In this solid conversion process, the π-π stacking behavior of growing graphene is spontaneously restrained, assisted by the gases produced simultaneously. Owing to the well-built three-dimensional (3D) framework structure and the oxygen-containing characteristic, the GFs have unique advantages in facilitating quasi-isotropic electron conduction, promoting ion transport and catalyzing molecule or ion reactions. These make the GFs display good electrode performance. In quantum dot sensitized solar cells (QDSSCs), the photovoltaic efficiency (η) for the GFs electrode is 3.57%, much higher than that (2.58%) for RGO electrode. In supercapacitor, the specific capacitance of the GFs electrode is 210 F $g^{-1}$ at current density of 0.5 A $g^{-1}$, which is much better than that of the RGO electrode (150 F $g^{-1}$).

In the first demonstration, 1.5 g of as-purchased solid sodium acetate (NaAc) particles (Figure 1b) loaded in a small ceramic boat were allowed to rapidly decompose in a tubular quartz reactor that was preheated to 1200 °C in argon stream (see Supplementary Materials and Methods). After a short-time reaction, typically one minute, the resulted black solids were moved out of the high-temperature zone and allowed to gradually cool to room temperature. Scanning electron microscopic (SEM) images show that the as-prepared product displays popcorn-like particles (Figure 1c), which usually link together by hundreds ones. The sizes (2-8

[a] State Key Laboratory of Coal Conversion, Institute of Coal Chemistry, Chinese Academy of Sciences, Taiyuan, 030001(China)
[b] University of Chinese Academy of Science, Beijing, 100049 (China)
* Address correspondence to zhengjf@sxicc.ac.cn ; zpzhu@sxicc.ac.cn
Electronic Supplementary Information (ESI) available: [details of any supplementary information available should be included here]. See DOI: 10.1039/x0xx00000x

μm) of the particles are several-fold the original NaAc sizes (1-3 μm), reflecting a significant volumetric expansion induced by the reaction. In the enlarged images, we observed the particle surfaces consist of thin graphene films, which display a fine framework structure (Figure 1d). Elemental analysis reveals that the particles also contain large amounts of sodium and oxygen atoms (Figure S1), which exist as a natrite structure of $Na_2CO_3$ crystals, as indicated by X-ray diffraction analysis (Figure S2). Accordingly, the as-prepared particles were washed with water fully to remove $Na_2CO_3$, and pure GFs were readily obtained. They display a hierarchy cellular structure, containing additional micrometer-scale macropores (Figure 1e), which are certainly left behind by the $Na_2CO_3$ removal. The observations by both transmission electron microscopy (TEM) and atomic force microscopy (AFM) reveal that the graphene has a few layers (Figures 1f and 1g).

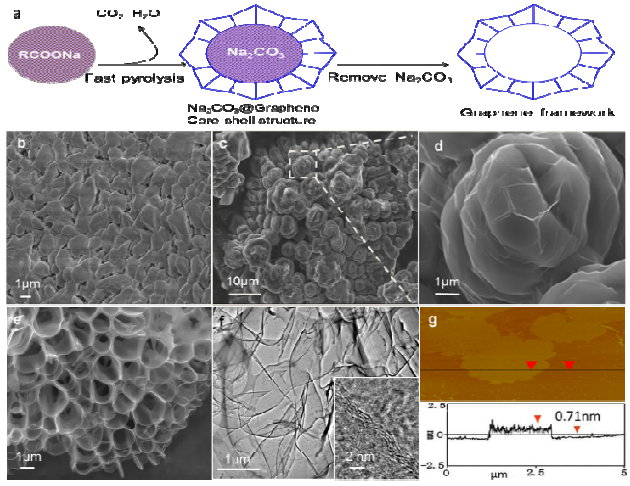


**Figure 1.** The formation of GFs. a, Schematic of the conversion of solid organic salt particles into GFs. b, SEM images of original NaAc particles. c, As-prepared popcorn-like GF particles with $Na_2CO_3$ cores, obtaining from a fast decomposition of NaAc particles at 1200 °C. d, A single GF particle enlarged. e, GFs purified by removing $Na_2CO_3$ cores. f, TEM image of the GFs. The inset is a typical HRTEM image. g, A representative AFM image of the GFs.

Raman spectrum of the GFs exhibits a $sp^2$-hybrid-characterized G band, a defect-derived D band, and a broad 2D band (Figure S3), similar to the spectra of the thermally or chemically reduced graphene oxides.[11,28,29] X-Ray Diffraction (XRD) pattern gives the obvious difference of GFs and graphite (Figure S4). X-ray photoelectron spectroscopy (XPS) reveals that about 8.8 at% of oxygen atoms are involved in the GFs and mainly structured as C-O single bonds (Figure S5), agreeing with the result from infrared analysis (Figure S6). The oxygen-containing characteristic is also similar to those obtained from the oxidation exfoliation of graphite and subsequent reduction.[30] It is beneficial to the functionalized modification and applications of graphene.[31-33] $N_2$ absorption measurement (Figure S7) shows that the GFs obtained from NaAc exhibits a BET special surface area of about 224.5 $m^2/g$. In addtion, the obtained GFs has good thermostability. After the post-annealing at 1200 °C for 1 h, the GFs still keeps its well-constructed framework structure (Figure S8).

Above data indicate that solid NaAc particles can be facilely converted into cellular graphene particles. Recently, there were some excellent reports on the synthesis of 3D graphene.[34-40] However, our method is quite different from those methods in many aspects. The detailed comparisons were given in Table S1. Compared with those methods, our method was simple, green, cheap and time-saving, which was quite possible to large scale synthesis and applications.

What is surprising is why the formed thin graphene films do not stack as bulk graphite crystals in such a circumstance with extremely high carbon density (about 35.4 $mmol/cm^3$ for NaAc). There must be a native power involved in the reaction system to resist the π-π interaction in real time. The power is likely associated with the gases ($CO_2$, CO, $H_2O$, $H_2$, and $CH_4$) formed continuously during the NaAc decomposition. In view of the thermal diffusion limitation within the micrometer-sized NaAc particles under the fast heating condition, predictably, the gas generation from NaAc decomposition and the graphene growth from carbon species would occur simultaneously in the short reaction duration. When gas generation rate (proportional to the rate of NaAc decomposition) is faster than the rate of gas diffusion, a local high-pressure environment would be created inside intermediate particles, in which growing graphene would be segregated in real time by an intercalation of the dense gases until they are cross linked and stabilized as 3D frameworks. This gas-mediated anti-stacking effect closely links with the expansion behaviour observed during the particle conversion and is somewhat analogous to the situation involved in the thermal exfoliation of graphite oxides reported previously,[28,29] where the quick decomposition of the rich oxygen-containing groups creates a transient high-pressure circumstance inside the graphite oxide particles, which drives graphite exfoliated as thin graphene films. More receivable evidences for the gas-mediated anti-stacking effect can be extracted from following the experimental observations.

Fast heating NaAc at high temperature, which majorly determines the rate of NaAc decomposition, is required for graphene formation. Although 2D carbon growth can be also achieved by a temperature-programmed (10 °C/min) gradual heating of NaAc particles, the resulted carbon sheets are heavily stacked, with thickness up to hundreds of nanometers (Figure S9). At relatively low temperatures such as 700 °C, carbons form only in a prolonged reaction time (about 4 min) under the fast heating condition and exhibit littery carbon debris as thick as tens nanometers (Figure S10). At temperatures above 800 °C, GFs can readily form (Figures S11, S12) and obviously show a thickness decline with increasing temperature (Figure 2a). This temperature effect can be well explained by the gas-mediated anti-stacking effect because temperature elevation speeds up NaAc decomposition and gas generation (Figure 2b, Figure S13), which will raise the local gas density and pressure inside intermediate particles and thus resist the inter-graphene stacking behaviour more efficiently.

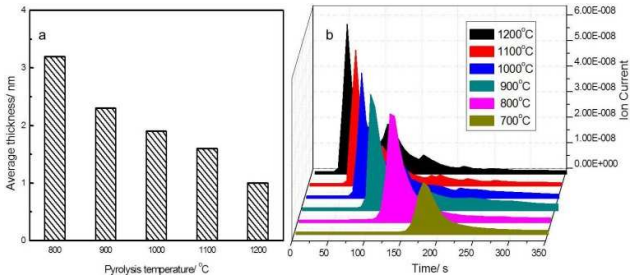


**Figure 2.** Dependence of NaAc decomposition temperature on (a) graphene thickness and (b) the release of $CO_2$, which was measured in real time by mass spectrometry at 44 amu fragments.

We also performed the fast decomposition of the solid particles of other organic sodium salts, such as propionate (NaPr), butyrate (NaBu), succinate (NaSu), and citrate (NaCi). For NaPr and NaBu, which have relatively lower content of -COO group and exhibit lower rate of gas generation in comparison with NaAc (Figure S14), the formation of thin graphene (Figure S15) requires higher temperatures such as 1200 °C to drive their decomposition and gas generation fast enough for an effective resistance to the π-π interaction. For NaSu and NaCi, which have relatively high content of -COO group and intrinsically can release more $CO_2$, they can be readily converted into uniform popcorn-like graphene particles (Figures 3a,b) even at relatively low temperatures such as 1000 °C, and pure cellular GFs can be obtained after a removal of the concomitant $Na_2CO_3$ (Figures 3c, d). These observations suggest a generality of the present direct solid conversion method for graphene synthesis and give additional support for the gas-mediated anti-stacking effect. Furthermore, we noticed that the sodium element involved in the starting material plays a crucial catalytic role in the graphene growth, at least, in the local fixing of carbon species as solid carbons because no solid product is left behind from the fast decomposition of the solid particles of succinic acid or citric acid under the same conditions.

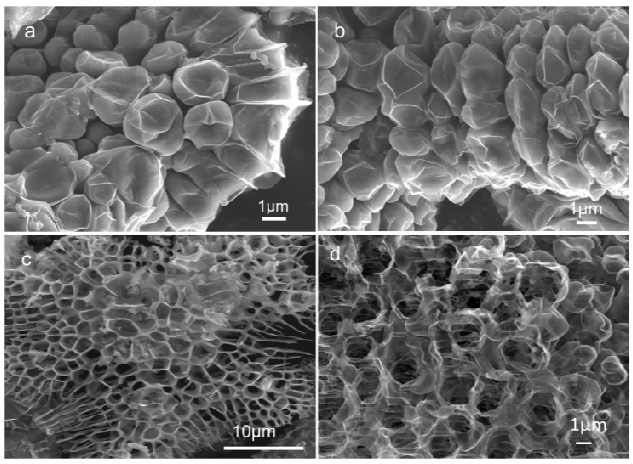


**Figure 3.** From NaSu and NaCi to GF particles. a, b, Popcorn-like GF particles as-prepared from fast decompositions of NaSu and NaCi, respectively. c, d, The GFs purified from the popcorn-like particles shown in a and b, respectively.

The practical application of graphene in condensed state requires an inhibition on their re-stacking behaviour, such as the morphologically modulation of them as curved or 3D framework structures.[29,34,36,41,42] Additional superiority of 3D GFs to the 2D counterpart can be found when they are used as functional electrodes such as those in solar cells and supercapacitors.[43-46] In QDSSCs, good conductivity, catalytic ability and ion transport ability of counter electrode (CE) are required to speed up the reduction of electrolyte ions, frequently $S_x^{2-}$ ion.[47-48] We have compared the GFs electrode with an electrode of 2D graphene (RGO, obtained from a chemical reduction of 2D graphene oxides[11]) in their impedance behaviour in $S^{2-}/S_x^{2-}$ electrolytes (Figure 4a), measured on symmetrical dummy cells comprising two identical electrodes (Figure S16). By fitting the Nyquist plots with an equivalent circuit model, the series resistance ($R_s$), charge transfer resistance ($R_{ct}$) at electrode-electrolyte interface, and Nernst diffusion impedance ($Z_N$) are extracted, as presented in Table S2. Obviously, the $R_{ct}$, and $Z_N$ values of the GFs electrode are both much lower than those of the RGO electrode, indicating the multiple promotion effects involved in the GFs. Unlike the anisotropic 2D graphene films that tend to arrange paralleling to electrode surface and display poor c-axis electron conduction, the 3D framework structure has a quasi-isotropic property and can provide multi-direction channels for electron conduction. Furthermore, the cellular structure of the GFs can greatly facilitate the diffusion of electrolyte ions and provides more accessible surfaces and active sites for the catalytic reduction of $S_x^{2-}$ ions, which closely correlates with its low $R_{ct}$ value.[43,49]

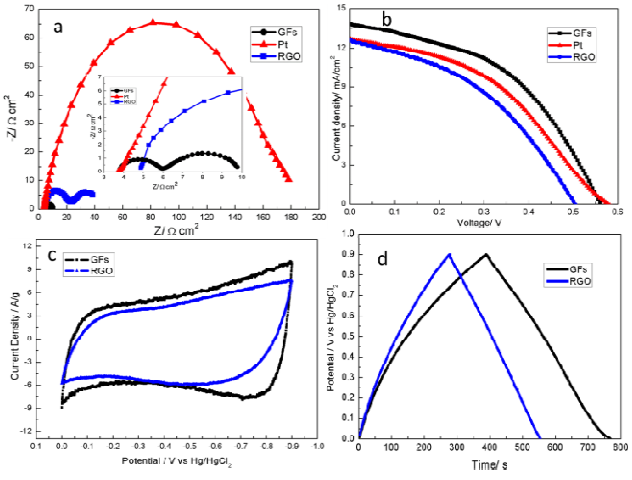


**Figure 4.** The electrochemical properties of GFs and RGO-modified electrodes. a, Nyquist plots of the symmetrical cells at a bias of 0.0 V under dark. Inset: the magnified version in high frequency region. b, Photocurrent density–voltage curves of the QDSSCs with GFs, RGO and Pt counter electrodes, measured at 100 mW·cm$^{-2}$ (AM 1.5). c, CV curves of GFs and RGO electrodes measured at 50 mV s$^{-1}$ in 6 M KOH. d, Galvanostatic charge–discharge curves of GFs and

RGO-modified electrodes at a current density of 0.5 A $g^{-1}$ in 6 M KOH.

The excellent basic properties of the GFs mean a potential greater than plane graphene as CE materials in QDSSCs system. As tested using packaged cells (see Supplementary materials and methods), the photovoltaic efficiency (η) for the GFs electrode is 3.57%, much higher than that (2.58%) for RGO electrode (Figure 4b, Table S2), similar to the situations reported previously.[37] Compared with the platinum (Pt) CE, the GFs electrode show a higher η and exhibit lower $R_{ct}$ and $Z_N$ (Table S2), revealing that the GFs electrode has excellent catalytic and ionic transport abilities for $S^{2-}/S_x^{2-}$ electrolyte, which makes it a promising candidate for counter electrode in QDSSCs.

Due to the framework structure, 3D graphene can also be favorable for the application in supercapacitors.[46-47] And therefore, the electrochemical energy storage performance of GFs electrode without conductive additive was studied. As shown in Figure 4c, compared with the the cyclic voltammetry (CV) curve of RGO-modified electrode, the CV curve of GFs-modified electrode had a better rectangular shape, indicading well capacitance behavior. The specific capacitance of the two kinds of electrodes were measured by galvanostatic charge/discharge test in a three-electrode system. As caculated from the discharging curve (Figure 4d), the specific capacitance of the GFs-modified electrode is 210 F $g^{-1}$at current density of 0.5 A $g^{-1}$, which is much better than that of the RGO-modified electrode (150 F $g^{-1}$). The improved capacitance behavior of GFs-modified electrode may be attributed to the framework structure of GFs, which can provide multi-direction channels for electron conduction and more transport pathways for the diffusion of electrolyte ions. This analysis can be verified by their impedance behavior (Figure S17 and Table S3). In addition, the GFs-modified electrode also displayed good cycling stability which retained over 92% of its capacitance over 2000 cycles at a current density of 2 A $g^{-1}$ (Figure S18).

## Conclusions

Summarily, we demonstrated that graphene with a cellular framework structure can be directly converted densely from solid organic salt particles by a quick thermal decomposition, during which the inherent inter-graphene π-π interaction is effectively restrained in real time by an intercalation effect of the large amount of gases produced locally. Although the graphene synthesized at the present stage are rich in structural defects, their unique cellular framework structure and the oxygen-containing characteristic, as demonstrated, endow them with unique advantages in facilitating quasi-isotropic electron conduction, promoting ion transport, and catalyzing molecule or ion reactions, which are intrinsically important in QDSSCs and supercapacitors. The η for the GFs electrode in QDSSCs is 3.57%, much higher than that (2.58%) for RGO electrode. The specific capacitance of the GFs electrode in supercapacitor is 210 F $g^{-1}$ at current density of 0.5 A $g^{-1}$, which is much better than that of the RGO-modified electrode (150 F $g^{-1}$). Particularly, overall consideration of the simple, green, cheap and time-saving synthesis method, the GFs is a promising and competitive electrode material. The knowledge on the gas-mediated anti-stacking effect might lead to new strategies for the syntheses of both graphene and other nanosheet materials.

## Notes and references

The authors gratefully acknowledge financial support from the Natural Science Foundation of Shanxi Province (2012011020-1) and Coal Base Key Scientific and Technological Program of Shanxi Province (MC2014-01).

1 K. S. Novoselov, V. I. Fal'ko, L. Colombo, P. R. Gellert, M. G. Schwab, K. Kim, *Nature,* 2012, **490**, 192.
2 V. Chabot, D. Higgins, A. Yu, X. Xiao, Z. Chen, J. Zhang, *Energy Environ. Sci.*, 2014, **7**, 1564.
3 S. Han, D. Wu, S. Li, F. Zhang and X. Feng, *Adv. Mater.*, 2014, **26**, 849.
4 B. Luo, S. Liu, L. Zhi, *Small,* 2012, **8**, 630.
5 Y. Li, G. Sheng, J. Sheng, *J. Mol. Liq.*, 2014, **199**, 474.
6 G. Zhao, J. Li, X. Ren, C. Chen, X. Wang, *Environ. Sci. Technol.*, 2011, **45**, 10454.
7 R. K. Upadhyay, N. Soin, S. S. Roy, *RSC Adv.* 2014, **4**, 3823.
8 K. S. Novoselov, A. K. Geim, S. V. Morozov, D. Jiang, Y. Zhang, S. V. Dubonos, I. V. Grigorieva, A. A. Firsov, *Science,* 2004, **306**, 666.
9 I. Y. Jeon, H. J. Choi, S. M. Jung, J. M. Seo, M. J. Kim, L. Dai, J. B. Baek, *J. Am. Chem. Soc.,* 2013, **135**, 1386.
10 Y. Hernandez, V. Nicolosi, M. Lotya, F. M. Blighe, Z. Sun, S. De, I. T. McGovern, B. Holland, M. Byrne, Y. K. Gun'Ko, J. J. Boland, P. Niraj, G. Duesberg, S. Krishnamurthy, R. Goodhue, J. Hutchison, V. Scardaci, A. C. Ferrari, J. N. Coleman, *Nat. Nanotechnol.,* 2008, **3**, 563.
11 S. Stankovich, D. A. Dikin, R. D. Piner, K. A. Kohlhaas, A. Kleinhammes, Y. Jia, Y. Wu, S. T. Nguyen, R. S. Ruoff, *Carbon,* 2007, **45**, 1558.
12 C. Berger, Z. Song, T. Li, X. Li, A. Y. Ogbazghi, R. Feng, Z. Dai, A. N. Marchenkov, E. H. Conrad, P. N. First, *J. Phys. Chem. B,* 2004, **108**, 19912.
13 T. Ohta, A. Bostwick, T. Seyller, K. Horn, E. Rotenberg, *Science,* 2006, **313**, 951.
14 X. Li, W. Cai, J. An, S. Kim, J. Nah, D. Yang, R. Piner, A. Velamakanni, I. Jung, E. Tutuc, S. K. Banerjee, L. Colombo, R. S. Ruoff, *Science,* 2009, **324**, 1312.
15 K. S. Kim, Y. Zhao, H. Jang, S. Y. Lee, J. M. Kim, K. S. Kim, J. H. Ahn, P. Kim, J. Y. Choi, B. H. Hong, *Nature,* 2009, **457**, 706.
16 Y. Lee, S. Bae, H. Jang, S. Jang, S.-E. Zhu, S. H. Sim, Y. I. Song, B. H. Hong, J.-H. Ahn, *Nano Lett.,* 2010, **10**, 490.
17 A. Reina, S. Thiele, X. Jia, S. Bhaviripudi, M. S. Dresselhaus, J. A. Schaefer, J. Kong, *Nano Res.,* 2009, **2**, 509.
18 Z. Sun, Z. Yan, J. Yao, E. Beitler, Y. Zhu, J. M. Tour, *Nature*, 2010, **468**, 549.
19 J. Cai, P. Ruffieux, R. Jaafar, M. Bieri, T. Braun, S. Blankenburg, M. Muoth, A. P. Seitsonen, M. Saleh, X. Feng, K. Mullen, R. Fasel, *Nature,* 2010, **466**, 470.
20 M. Treier, C. A. Pignedoli, T. Laino, R. Rieger, K. Müllen, D. Passerone, R. Fasel, *Nat. Chem.,* 2011, **3**, 61.
21 L. Qu, Y. Liu, J.-B. Baek, L. Dai, *ACS Nano,* 2010, **4**, 1321.
22 Y. Z. Tan, B. Yang, K. Parvez, A. Narita, S. Osella, D. Beljonne, X. Feng, K. Mullen, *Nat. Commun.,* 2013, **4**, 2646.
23 F. Bonaccorso, Z. Sun, T. Hasan, A. Ferrari, *Nat. Photonics,* 2010, **4**, 611.
24 J. R. Miller, R. Outlaw, B. Holloway, Science, 2010, **329**, 1637.
25 R. Kou, Y. Shao, D. Mei, Z. Nie, D. Wang, C. Wang, V. V. Viswanathan, S. Park, I. A. Aksay, Y. Lin, *J. Am. Chem. Soc.,* 2011, **133**, 2541.
26 J. Kang, D. Shin, S. Bae, B. H. Hong, *Nanoscale,* 2012, **4**, 5527.

27 L. Gao, G.-X. Ni, Y. Liu, B. Liu, A. H. Castro Neto, K. P. Loh, *Nature,* 2013, **505**, 190.
28 H. C. Schniepp, J.-L. Li, M. J. McAllister, H. Sai, M. Herrera-Alonso, D. H. Adamson, R. K. Prud'homme, R. Car, D. A. Saville, I. A. Aksay, *J. Phys. Chem. B,* 2006, **110**, 8535.
29 J. Yan, J. Liu, Z. Fan, T. Wei, L. Zhang, *Carbon,* 2012, **50**, 2179.
30 S. Dubin, S. Gilje, K. Wang, V. C. Tung, K. Cha, A. S. Hall, J. Farrar, R. Varshneya, Y. Yang, R. B. Kaner, *ACS Nano,* 2010, **4**, 3845.
31 T. Y. Kim, H. W. Lee, M. Stoller, D. R. Dreyer, C. W. Bielawski, R. S. Ruoff, K. S. Suh, *ACS Nano,* 2010, **5**, 436.
32 Y. Xu, Z. Liu, X. Zhang, Y. Wang, J. Tian, Y. Huang, Y. Ma, X. Zhang, Y. Chen, *Adv. Mater.,* 2009, **21**, 1275.
33 Y. Xu, L. Zhao, H. Bai, W. Hong, C. Li, G. Shi, *J. Am. Chem. Soc.,* 2009, **131**, 13490.
34 Z.P. Chen, W.C. Ren, L.B. Gao, B.L. Liu, S.F. Pei, H.M. Cheng, *Nat. Mater.*, 2011,**10**, 424.
35 Z. S. Wu, Y. Sun, Y. Z. Tan, S. Yang, X. Feng, K. Mullen, *J.Am. Chem. Soc.,* 2012, **134**, 19532.
36 Y. Zhao, C. Hu, Y. Hu, H. Cheng, G. Shi, L. Qu, *Angew. Chem. Int. Ed.,* 2012, **51**, 11371.
37 C. M. Chen, Q. Zhang, C. H. Huang, X. C. Zhao, B. S. Zhang, Q. Q. Kong, M. Z. Wang, Y. G. Yang, R. Cai, D. Sheng Su, *Chem. Commun.*, 2012, **48**, 7149.
38 B. G. Choi, M. Yang, W. H. Hong, J. W. Choi, Y. S. Huh, *ACS Nano.*, 2012, **6**, 4020.
39 Y. Jiao, D. Han, L. Liu, L. Ji, G. Guo, J. Hu, D. Yang, A. Dong, *Angew. Chem. Int. Ed.,* 2015, **54**, 5727.
40 Y. Jiao, D. Han, Y. Ding, X. Zhang, G. Guo, J. Hu, D. Yang, A. Dong, *Nat. Commun.,* 2015, **6**, 6420.
41 X. Wang, Y. Zhang, C. Zhi, X. Wang, D. Tang, Y. Xu, Q. Weng, X. Jiang, M. Mitome, D. Golberg, *Nat. Commun.,* 2013, **4,** 2905.
42 L. Qiu, J. Z. Liu, S. L. Chang, Y. Wu, D. Li, *Nat. Commun.,* 2012, **3**, 1241.
43 H. Wang, K. Sun, F. Tao, D. J. Stacchiola, Y. H. Hu, *Angew. Chem. Int. Ed. ,* 2013, **52**, 9210.
44 J. S. Lee, H. J. Ahn, J. C. Yoon, J. H. Jang, *Phys. Chem. Chem. Phys.,* 2012, **14**, 7938.
45 H. S. Ahn, J. W. Jang, M. Seol, J. M. Kim, D. J. Yun, C. Park, H. Kim, D. H. Youn, J. Y. Kim, G. Park, S. C. Park, J. M. Kim, D. I. Yu, K. Yong, M. H. Kim, J. S. Lee, *Sci. Rep.,* 2013, **3**, 1396.
46 J. Hu, Z. Kang, F. Li and X. Huang, *Carbon,* 2014, **67**, 221.
47 Z. Yang, C.Y. Chen, C.W. Liu, H.T. Chang, *Chem. Commun.,* 2010, **46**, 5485.
48 J. G. Radich, R. Dwyer, P. V. Kamat, J. Phys. *Chem. Lett.,* 2011, **2**, 2453.
49 F. Gong, H. Wang, X. Xu, G. Zhou, Z. S. Wang, *J. Am. Chem. Soc.,* 2012, **134**, 10953.